World Journal of Radiology

Submit a Manuscript: https://www.f6publishing.com

World J Radiol 2023 April 28; 15(4): 98-117

DOI: 10.4329/wjr.v15.i4.98

ISSN 1949-8470 (online)

MINIREVIEWS

Evaluation of causal heart diseases in cardioembolic stroke by cardiac computed tomography

Shu Yoshihara

Specialty type: Cardiac and cardiovascular systems

Provenance and peer review: Invited article; Externally peer reviewed.

Peer-review model: Single blind

Peer-review report's scientific quality classification

Grade A (Excellent): 0
Grade B (Very good): B, B, B
Grade C (Good): 0
Grade D (Fair): 0
Grade E (Poor): 0

P-Reviewer: Gupta P, United States; Liao X, China; Ong H, Malaysia

Received: December 6, 2022
Peer-review started: December 6, 2022
First decision: March 1, 2023
Revised: March 8, 2023
Accepted: March 30, 2023
Article in press: March 30, 2023
Published online: April 28, 2023

Shu Yoshihara, Department of Diagnostic Radiology, Iwata City Hospital, Iwata 438-8550, Shizuoka, Japan

Corresponding author: Shu Yoshihara, MD, PhD, Doctor, Department of Diagnostic Radiology, Iwata City Hospital, 512-3 Ookubo, Iwata 438-8550, Shizuoka, Japan.
shuy@hospital.iwata.shizuoka.jp

Abstract

Cardioembolic stroke is a potentially devastating condition and tends to have a poor prognosis compared with other ischemic stroke subtypes. Therefore, it is important for proper therapeutic management to identify a cardiac source of embolism in stroke patients. Cardiac computed tomography (CCT) can detect the detailed visualization of various cardiac pathologies in the cardiac chambers, interatrial and interventricular septum, valves, and myocardium with few motion artifacts and few dead angles. Multiphase reconstruction images of the entire cardiac cycle make it possible to demonstrate cardiac structures in a dynamic manner. Consequently, CCT has the ability to provide high-quality information about causal heart disease in cardioembolic stroke. In addition, CCT can simultaneously evaluate obstructive coronary artery disease, which may be helpful in surgical planning in patients who need urgent surgery, such as cardiac tumors or infective endocarditis. This review will introduce the potential clinical applications of CCT in an ischemic stroke population, with a focus on diagnosing cardioembolic sources using CCT.

Key Words: Acute ischemic stroke; Cardioembolic stroke; Cardiac computed tomography

Core Tip: Cardiac computed tomography (CCT) can detect the detailed visualization of causal heart disease in cardioembolic stroke. This review introduces the potential clinical applications of CCT in an ischemic stroke population, with a focus on diagnosing cardioembolic sources using CCT. Specifically, left atrial thrombus and associated pathologies, left ventricular thrombus and associated pathologies, intracardiac tumors, valvular abnormalities, and causal pathologies of paradoxical embolism are discussed.

Citation: Yoshihara S. Evaluation of causal heart diseases in cardioembolic stroke by cardiac computed tomography. *World J Radiol* 2023; 15(4): 98-117
URL: https://www.wjgnet.com/1949-8470/full/v15/i4/98.htm
DOI: https://dx.doi.org/10.4329/wjr.v15.i4.98

INTRODUCTION

Ischemic stroke is a sudden onset of a focal neurologic deficit attributed to cerebral ischemia that results in neuron death. Ischemic stroke is etiologically sub-classified into four categories: Large artery atherosclerosis, cardiac embolism, small vessel occlusion, and other uncommon causes[1,2]. Ischemic stroke due to cardiac embolism commonly has a sudden onset, is more prone to hemorrhagic transformation, and generally carries a worse prognosis with respect to disability, mortality, and early and long-term recurrence of stroke compared with other etiologies. Therefore, in the diagnostic work-up of ischemic stroke patients with suspected embolism, identification of a cardioembolic source is essential in determining appropriate secondary prevention. The diagnosis of cardioembolic stroke is usually performed based on medical history information, physical examination, laboratory testing, 12-lead electrocardiogram (ECG), heart rhythm monitoring (in-hospital telemetry, ambulant 24-h Holter), and transthoracic echocardiography (TTE)[3]. Transesophageal echocardiography (TEE) is highly accurate in the detection of abnormalities in the left atrium and left atrial appendage (LAA), atrial septum, mitral valve, and aortic arch. In fact, TEE has been shown to be superior to TTE for detecting potential sources of cardiac embolism in patients with ischemic stroke[4,5]. However, TEE has inherent associated risks, including esophageal injury, aspiration, and hypertension or hypotension during the procedure. Although TEE complication rates are very low, TEE may be difficult to perform in stroke patients with neurologic deficits that make it impossible to cooperate with instructions given during the procedure. Progress in the technical development of cardiac computed tomography (CCT) enables rapid, accurate imaging of the cardiovascular system. With CCT, it is necessary to use either prospective or retrospective ECG gating to synchronize the CT image with the ECG. In both methods, the ECG waveform is used to coordinate image reconstruction with the heart's position in the chest. The diagnostic accuracy of CCT compared with invasive coronary angiography has been evaluated in multiple trials. A meta-analysis across nine studies identified 97% sensitivity with 78% specificity for detecting > 50% stenosis[6]. In addition to stenosis location and severity, CCT can simultaneously evaluate the plaque characteristics and plaque burden of the coronary artery (Table 1). With its high spatial resolution and multiplanar reconstruction capabilities, CCT can detect the detailed visualization of various cardiac pathologies in the cardiac chambers, interatrial and interventricular septum, valves, and myocardium with few motion artifacts and few dead angles. In addition, multiphase reconstruction images of the entire cardiac cycle detected by retrospective ECG gating can provide a functional assessment of cardiac structure in a dynamic manner (Cine-CT)[7]. Therefore, CCT has the ability to provide high-quality information about causal heart disease in cardioembolic stroke. Indeed, current guidelines indicate that CCT should be performed as a second step if echocardiography is non-diagnostic in evaluating cardiac mass, valvular heart disease, and congenital heart disease[8].

This review will introduce the potential clinical applications of CCT in an ischemic stroke population, with a focus on diagnosing cardioembolic sources using CCT.

CARDIOEMBOLIC SOURCES OF ISCHEMIC STROKE

Numerous cardiac conditions have been proposed as potential sources of embolism. Based on the evidence of their relative propensities for embolism, cardiac sources are divided into two categories: High risk and medium risk (Table 2). Compared to standard stroke management, patients at high risk for cardioembolic stroke require a different therapeutic strategy, such as the prescription of anticoagulants. Patients at medium risk for cardioembolic stroke exhibit a strong association with increased risk of stroke, but currently there are no clear and appropriate management guidelines for the prevention of stroke occurrence. Cardiac sources of embolism are classified into arrhythmias and structural cardiac diseases. Atrial fibrillation (Af) is the most common arrhythmia related to embolic stroke. Atrial flutter and sick sinus syndrome (tachycardia-bradycardia syndrome) are also associated with a higher risk of stroke. The diagnosis of atrial dysrhythmias is performed by 12-lead ECG and heart rhythm monitoring (in-hospital telemetry, 24-h Holter ECG, prolonged rhythm monitoring). Structural cardiac diseases are usually diagnosed by echocardiography. CCT can provide complementary information to echocardiography in the diagnosis of structural cardiac sources of embolism.

Table 1 Information suitable for detection by cardiac computed tomography

Condition	Location	Information
Coronary artery disease	Coronary artery	Stenosis location and severity
		Plaque characteristics
		Plaque burden: CAC score, plaque volume
		Other: Pericoronary FAI, FFR_{CT}
	Myocardium	Enhancement pattern: Perfusion defect, LIE
		Degeneration: Fat, calcification, wall thinning
	Wall motion	Regional wall motion abnormality: LV, RV
		Global function: LV, RV
Valvular heart disease	Native heart valve	Aortic stenosis: BAV or TAV, AVA, pre and post evaluation of TAVR
		Chronic secondary mitral regurgitation: Etiology assessment
		Calcium score: AV, MAC
	Prosthetic heart valve	Mechanical valve dysfunction
	Infective endocarditis	Periannular complication
Congenital heart disease		Anomaly of coronary artery
		Anomaly of thoracic arteriovenous vessels
		Complex and repaired adult congenital heart disease
		Unusual anatomy of atrial and ventricular septal defect
		Quantitative evaluation of right ventricular function

CAC: Coronary artery calcium; FAI: Fat attenuation index; FFR_{CT}: CT-derived fractional flow reserve; LIE: Late iodine enhancement; LV: Left ventricle; RV: Right ventricle; BAV: Bicuspid aortic valve; TAV: Tricuspid aortic valve; AVA: Aortic valve area; TAVR: Transcatheter aortic valve replacement; AV: Aortic valve; MAC: Mitral annular calcification.

CARDIAC CT FOR DIAGNOSIS OF SPECIFIC CARDIOEMBOLIC SOURCES

Left atrial thrombus and associated pathologies

Stroke associated with Af is attributed to embolism of thrombus from the left atrium (LA). The LAA is an anterolateral muscular extension of the LA arising adjacent to the left superior pulmonary vein and lying in the left atrioventricular sulcus close to the left circumflex coronary artery. The LAA is an embryological remnant that functions as a reservoir during conditions of fluid overload. Because of its hooked morphology, blood stasis tends to occur in the LAA. As a result, more than 90% of thrombi in patients with Af originate from the LAA[9]. Structural and functional aspects of the LAA are linked to stroke risk in patients with Af. For example, stasis resulting from decreased emptying of the LAA due to loss of organized mechanical contraction during the cardiac cycle, as evidenced by reduced LAA flow velocities on TEE, is associated with thrombus formation and stroke risk.

In CCT examination under sinus rhythm, the LAA is opacified with a contrast medium in the early phase, which evaluates the coronary artery. By contrast, in CCT examination under atrial fibrillation, a contrast medium filling defect is usually observed in the LAA, which reflects the stasis of blood flow within the LAA. A contrast medium filling defect in the LAA is an important finding by itself. In patients with Af, increased contrast heterogeneity within the LAA on contrast-enhanced CT correlates with an increased degree of spontaneous echo contrast and decreased LAA emptying velocity on TEE [10-12]. Furthermore, in a study of 1019 patients who underwent CCT before first-time radiofrequency catheter ablation for Af, Kawaji *et al*[13] reported that patients with severe contrast medium filling defects in the LAA are associated with higher incidence of ischemic stroke compared to patients with mild or no filling defects in the LAA during a mean follow-up of 4.4 years. However, the assessment of thrombi in the LAA is confounded by such filling defects. Therefore, a second scan should be performed several minutes after the initial first-pass scan. The addition of delayed imaging enables a better distinction of both thrombus and blood stasis. An apparent filling defect in the LAA observed in early phase resolves in delayed phase if no thrombus is present (Figure 1). On the other hand, true thrombi in the LAA can be recognized as a filling defect in both early and delayed phases (Figure 2). In a meta-analysis of seven studies with a total of 753 patients for whom delayed images were obtained, CCT

Table 2 Sources of cardioembolism

Risk level	Source	Condition
High-risk sources	Left atrial thrombus	Atrial fibrillation (Af)
		Mitral valve stenosis
	Left ventricular thrombus	Acute myocardial infarction
		Cardiomyopathy (ischemic, nonischemic)
		Congestive heart failure with low ejection fraction
	Cardiac tumor	Primary cardiac tumor
		Secondary cardiac tumor
	Vegetation	Infective endocarditis
		Nonbacterial thrombotic endocarditis
	Mechanical prosthetic heart valve	
Medium-risk sources	Interatrial septal abnormalities	Patent foramen ovale
		Atrial septal aneurysm
		Atrial septal defect
	Interventricular septal abnormalities	Interventricular membranous septal aneurysm
		Ventricular septal defect
	Pulmonary arteriovenous malformation	
	Bioprosthetic heart valve	
	Valvular abnormalities other than tumor and vegetation	Aortic valve sclerosis/stenosis
		Mitral annular calcification
		Lambl's excrescences
		Calcified amorphous tumor
		Mitral valve prolapse
	Atrial cardiomyopathy	
	Atrial arrhythmias other than Af	Atrial flutter
		Sick sinus syndrome

showed equivalent diagnostic accuracy as TEE for detecting LA/LAA thrombus in patients with Af. Specifically, two-phase CCT yielded sensitivity, specificity, positive predictive value, and negative predictive value of 100%, 99%, 92%, and 100%, respectively, compared with TEE as a reference standard [14]. Although the LAA is the most frequent site of atrial thrombi, they can occur in the right atrial appendage or in the atrial chambers themselves, especially in the context of Af and/or significant valvular heart disease such as mitral and tricuspid stenoses (Figure 3).

Among all native valvular heart disease, the risk of systemic emboli is highest for rheumatic mitral valve disease. Compared to normal controls, Af with rheumatic heart disease is associated with a 17-fold increase in stroke incidence, whereas it is five-fold for Af in the absence of RHD[15]. The risk of embolization is higher for mitral stenosis than mitral regurgitation, and the risk of embolism increases approximately seven-fold in the presence of Af compared to those with sinus rhythm in patients with rheumatic mitral valve disease[16]. In addition to delineating the morphological abnormalities of the mitral valve apparatus, CCT can comprehensively evaluate LA function and the presence or absence of LAA thrombus in a single examination (Figure 4).

LAA size is associated with increased thromboembolic risk[17,18]. Veinot *et al*[19] studied 500 normal autopsy hearts, and reported the size of normal LAAs differentiated by age group and sex. Mean LAA orifice diameter, body width, and length in subjects aged 20 or older were, respectively, 1.16, 1.83, and 2.59 cm for men and 1.07, 1.66, and 2.53 cm for women. Figure 5 shows a case of LAA aneurysm. Although a clear consensus on a definition of LAA aneurysm does not exist, Aryal *et al*[20] proposed defining it as a LAA with dimensions larger than 2.7 cm in orifice diameter, 4.8 cm in body width, and 6.75 cm in length. Whether congenital or acquired, LAA aneurysms grow in size over several years, and they tend to become symptomatic with an increasing risk of thromboembolism. Thus, surgical treatment for LAA aneurysm is often recommended, even in asymptomatic patients. By reconstructing images of

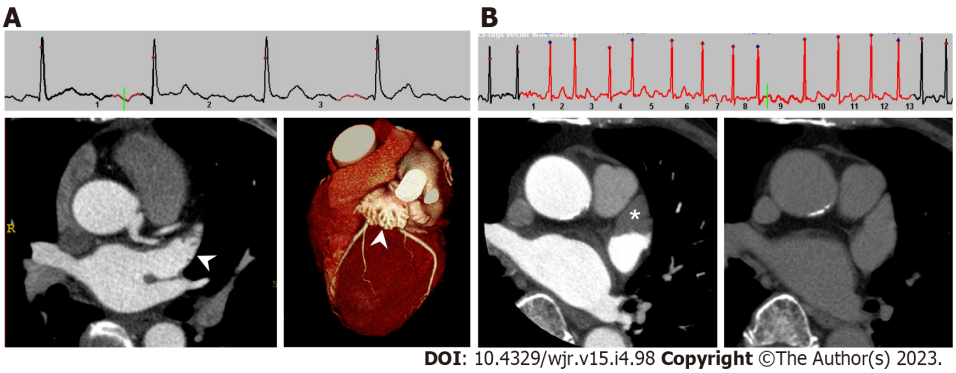

DOI: 10.4329/wjr.v15.i4.98 Copyright ©The Author(s) 2023.

Figure 1 Cardiac computed tomography images of left atrial appendage in patients with sinus rhythm and atrial fibrillation. A: Under normal sinus rhythm, left atrial appendage (LAA) is filled with contrast medium in early phase, which evaluates the coronary artery. Left: axial image; right: three-dimensional volume-rendered image; B: Under atrial fibrillation, axial early phase image shows triangular filling defect in LAA (left, asterisk). On delayed phase (right), LAA filling defect completely disappeared, which means the filling defect reflected blood stasis in LAA rather than thrombus.

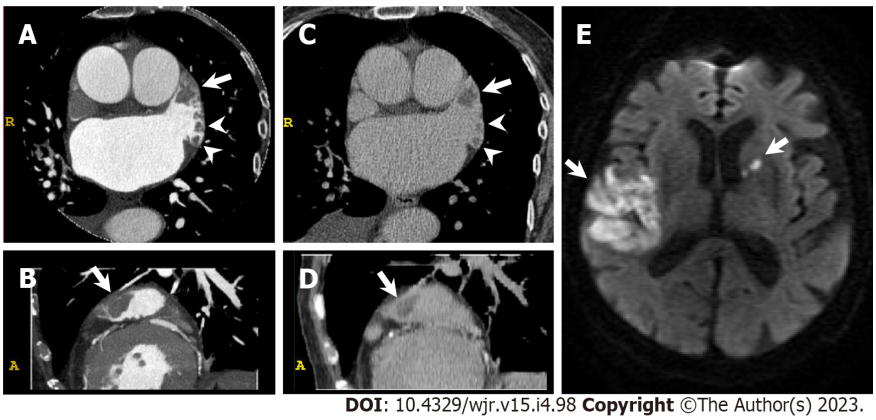

DOI: 10.4329/wjr.v15.i4.98 Copyright ©The Author(s) 2023.

Figure 2 Left atrial appendage thrombus. An 85-year-old woman with congestive heart failure and atrial fibrillation underwent cardiac computed tomography (CCT) in search of underlying heart disease. She suffered from acute ischemic stroke three months after CCT. A and B: Early phase CCT images (A: Axial; B: Sagittal) show multiple filling defects in left atrial appendage (LAA, arrow and arrowheads); C and D: Delayed phase CCT images (C: Axial; D: Sagittal) also show multiple filling defects in LAA (arrow and arrowheads) confirming multiple LAA thrombus; E: Diffusion-weighted brain magnetic resonance imaging shows hyperintense lesions in right temporoparietal lobe and left anterior limb of internal capsule (arrows).

multiple phases throughout the cardiac cycle acquired by retrospective ECG gating, CCT can accurately quantify the volumes of cardiac chambers and calculate ventricular and atrial ejection fraction. The average maximum volume of the LAA on CCT in subjects with sinus rhythm and no history of cardiac disease was reported to be 12.54 mL for men and 11.74 mL for women[21]. In the presented case of LAA aneurysm, the CCT-derived maximum LAA volume was 56 mL (Figure 5).

Based on the imaging characteristics, the shapes of the LAA are classified into four different categories: chicken-wing, cactus, windsock, and cauliflower[22]. There is growing evidence that the morphology of the LAA delineated by CCT can assist with risk stratification in patients with nonvalvular Af. Specifically, patients with non-chicken-wing LAA morphology are significantly more likely to experience thromboembolic events than patients with chicken-wing LAA morphology[9]. Moreover, with regard to the cauliflower LAA morphology, defined as a main lobe less than 4 cm long and without forked lobes, Kimura *et al*[23] demonstrated that it was significantly more common in patients with stroke.

Left ventricular thrombus and associated pathologies

Left ventricular (LV) thrombus is complicated with various cardiac diseases that impair LV wall motion and can induce thromboembolic complications such as stroke. Causal pathologies that generate LV thrombus are classified into acute disorders and chronic disorders. Acute myocardial infarction (AMI) is a representative acute disorder. Prolonged myocardial ischemia results in subendocardial and endothelial injury and increased concentration of procoagulant factors, whereas akinetic areas of necrotic myocardium lead to blood stasis, especially at the LV apex. In data from the era without early coronary reperfusion therapy for AMI, LV thrombus was present in 46% of patients, usually in the first two weeks after onset, and most frequently in acute anterior or apical MI[24]. Although the frequency of LV thrombus in AMI has been significantly lowered since the advent of primary percutaneous coronary

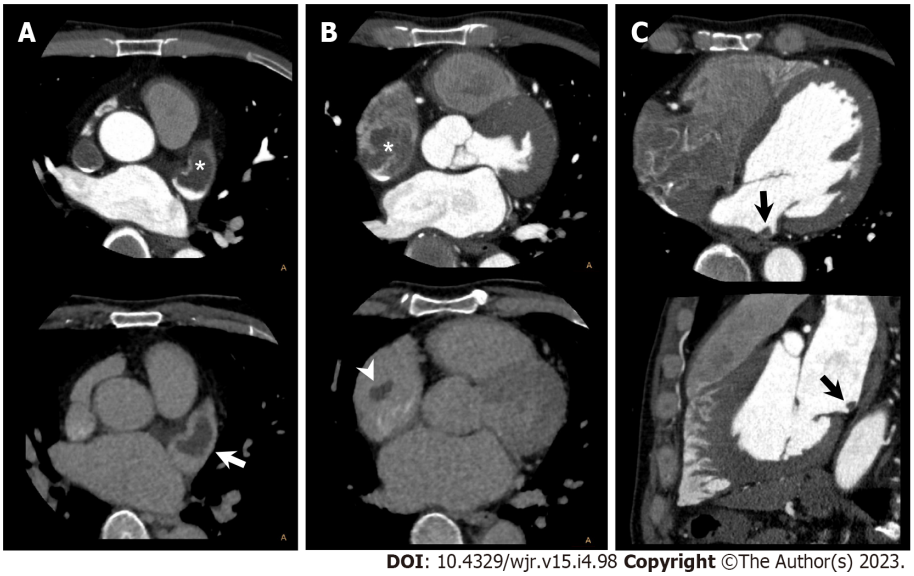

DOI: 10.4329/wjr.v15.i4.98

Figure 3 Bilateral atrial thrombus. A 53-year-old man with atrial fibrillation and right renal infarction underwent cardiac computed tomography (CCT) in search of causal heart pathology of cardioembolism. A: Axial early phase CCT image shows filling defect in left atrial appendage (LAA, upper, asterisk). Axial delayed phase CCT image also shows filling defect in LAA confirming LAA thrombus (lower, arrow); B: Axial early phase CCT image shows filling defect in right atrial appendage (RAA, upper, asterisk). Axial delayed phase CCT image also shows filling defect in RAA confirming RAA thrombus (lower, arrowhead); C: Early phase CCT images (upper: Axial; lower: Sagittal) show filling defect in LA posterior wall, which suggests LA thrombus (black arrow).

intervention and dual antiplatelet therapy, the predilection site of LV thrombus has not changed and most frequently occurs in patients with acute anterior or apical MI[25]. Patients with MI also have a long-term risk of stroke after the acute phase. In the Survival and Ventricular Enlargement study, the cumulative rate of stroke risk was 8.1% during the five years after MI, and a lower LV ejection fraction (EF) was the independent predictor of stroke[26]. Specifically, patients with LVEF values of 35% or more and 28% or less had a cumulative stroke rate of 4.1% and 8.9%, respectively. Weinsaft *et al*[27] used cardiac magnetic resonance imaging (MRI) in 784 patients with LV systolic dysfunction (LVEF values of 50% or less), predominantly of chronic MI, and found the prevalence of thrombus to be 7% in this population. Patients with thrombus were more likely to have LV aneurysms, lower LVEF, and more extensive myocardial scarring by delayed enhanced MRI. Figure 6 shows a case of acute ischemic stroke due to LV apical thrombus complicated with chronic anteroseptal MI. In CCT, because the LV endocardial border is clearly depicted, LV thrombus is easily detected as a hypodense mass within the contrast-enhanced LV cavity. When blood stasis within the left ventricle disturbs the visibility of LV thrombus in the early phase image, a second scan should be performed several minutes after the initial first-pass scan. The addition of delayed imaging enables a better distinction of both thrombus and blood stasis. The LV apex is one of the anatomical blind spots at TTE[28]. Especially, when the LV apex becomes aneurysmal, the finding tends to be missed at TTE because the true apex often extends beyond its usual visualized location. Indeed, the diagnostic performance of TTE for detecting LV thrombus is inferior compared with cardiac MRI[29]. Takotsubo syndrome is also an acute disorder that generates LV thrombus. Takotsubo syndrome, caused in part by sympathetic activation and excess catecholamines, leads to LV apical ballooning, global or focal LV and/or right ventricular wall motion abnormalities, and increased risk of stroke and TIA[30].

A representative chronic disorder that generates LV thrombus is cardiomyopathy. In patients with cardiomyopathy, annual stroke rates are reported to be in the range of 1.3% to 3.5%[31]. The risk of stroke is inversely related to LVEF in patients with cardiomyopathy, whether its etiology is ischemic or nonischemic[31]. Risk factors that predispose patients with cardiomyopathies to thromboembolic events include extensive LV wall motion abnormalities, very dilated left ventricles, low cardiac output with the stagnation of blood within the ventricle, significant slow swirling streaks of blood within the left ventricle, and the presence of Af. Figure 7 shows a case of LV noncompaction. LV noncompaction is a rare congenital cardiomyopathy caused by an arrest of myocardial morphogenesis that results in prominent endomyocardial trabeculations in the LV myocardium. Deep myocardial recesses are thought to aggravate the risk of ventricular thrombus formation. Because thromboembolic risk is recognized to be high, anticoagulation should be considered in patients with LV noncompaction[32].

Figure 8 shows a case of mid-ventricular obstructive hypertrophic cardiomyopathy (HCM) with LV apical aneurysm and LV apical thrombus. In HCM, the location and degree of hypertrophy are variable. Although asymmetric septal hypertrophy is the classic and most common morphologic subtype of HCM, hypertrophy can involve various LV segments and may be focal or concentric. Mid-ventricular obstructive HCM is an uncommon type of HCM and is complicated with LV apical aneurysms in more

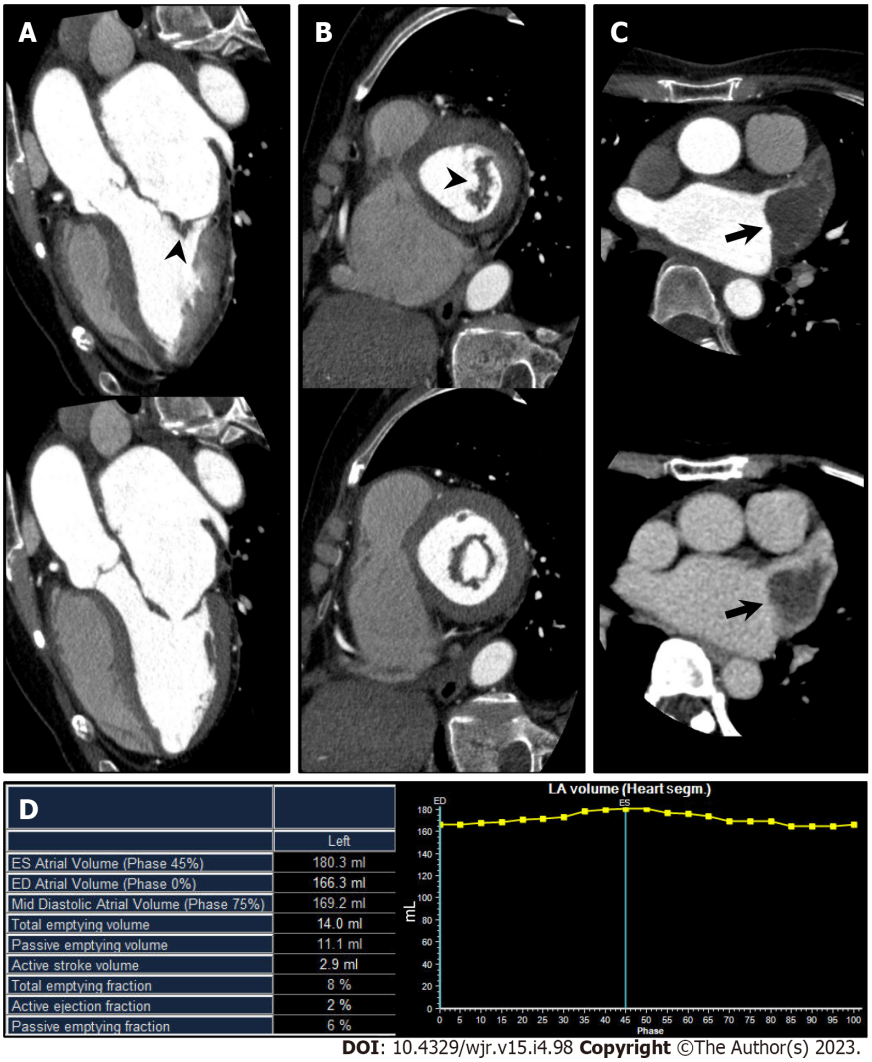

DOI: 10.4329/wjr.v15.i4.98

Figure 4 Mitral stenosis. A 70-year-old man with mitral stenosis and atrial fibrillation underwent cardiac computed tomography (CCT) to rule out obstructive coronary artery disease. A and B: Left ventricular outflow tract long axis (A) and short axis (B) reformatted CCT images (upper: Mid systole at 20% of the R-R interval; lower: Mid diastole at 80% of the R-R interval) show thickened anterior and posterior mitral valve leaflets (arrowhead) and restricted mitral valve opening, representing mitral stenosis. Associated severe enlargement of left atrium is also found; C: Axial early phase CCT image shows triangular filling defect in left atrial appendage (LAA, upper, arrow). Axial delayed phase CCT image also shows filling defect in LAA confirming LAA thrombus (lower, arrow); D: Atrial functional analysis shows severely impaired LA function. LA end-systolic volume, end-diastolic volume, and ejection fraction were 180.3 mL, 166.3 mL, and 8%, respectively.

than 20% of cases of this phenotype[33]. In patients with HCM, the presence of LV apical aneurysm increases the risk for thromboembolic events six-fold compared with HCM patients without LV apical aneurysm[34].

Figure 9 shows a case of interventricular membranous septal aneurysm (IVMSA). Because the membranous portion of the interventricular septum notably lacks myocardium, this structure predisposes to the development of IVMSA upon exposure to a high-pressure gradient. The blood stasis in this abnormal structure predisposes to thrombus formation within the IVSMA. Although IVMSA is a rare condition, it can be one of the causal pathologies of LV thrombus and a potential source of cardioembolic stroke[35].

Intracardiac tumors

Cardiac tumors are classified into primary and secondary tumors. Primary cardiac tumors are very rare, and secondary or metastatic cardiac tumors are 30 times more common[36]. The affected cardiac chamber of predilection is different among cardiac tumor subtypes. Cardiac tumors that affect left heart chambers and valves provoke systemic thromboembolic phenomena. Tumor fragment detachment or superimposed thrombi underlie embolic risk. A representative cardiac tumor that induces embolic stroke is cardiac myxoma (Figure 10 and 11), which is the most frequent primary cardiac neoplasm in adults. Cardiac myxomas are most commonly found within the left atrium but may arise from other cardiac chambers and rarely from the valves. Although they are histologically benign, they can provoke potentially life-threatening conditions like thromboembolic phenomena or intracardiac obstructive complications. Neurologic complications can be the first manifestation of cardiac myxoma[37,38]. For

DOI: 10.4329/wjr.v15.i4.98 **Copyright** ©The Author(s) 2023.

Figure 5 Left atrial appendage aneurysm. A 56-year-old man with atrial fibrillation (Af) underwent cardiac computed tomography (CCT) to rule out obstructive coronary artery disease before catheter ablation for Af. A and B: Axial (A) and sagittal (B) reformatted CCT images show enlarged left atrial appendage (LAA, arrow) with triangular filling defect inside. LAA orifice diameter, body width, and length were 3.4 cm, 5.2 cm, and 6.8 cm, respectively; C: Three-dimensional volume-rendered image of CCT shows LAA aneurysm. CCT-derived maximum LAA volume was 56 mL.

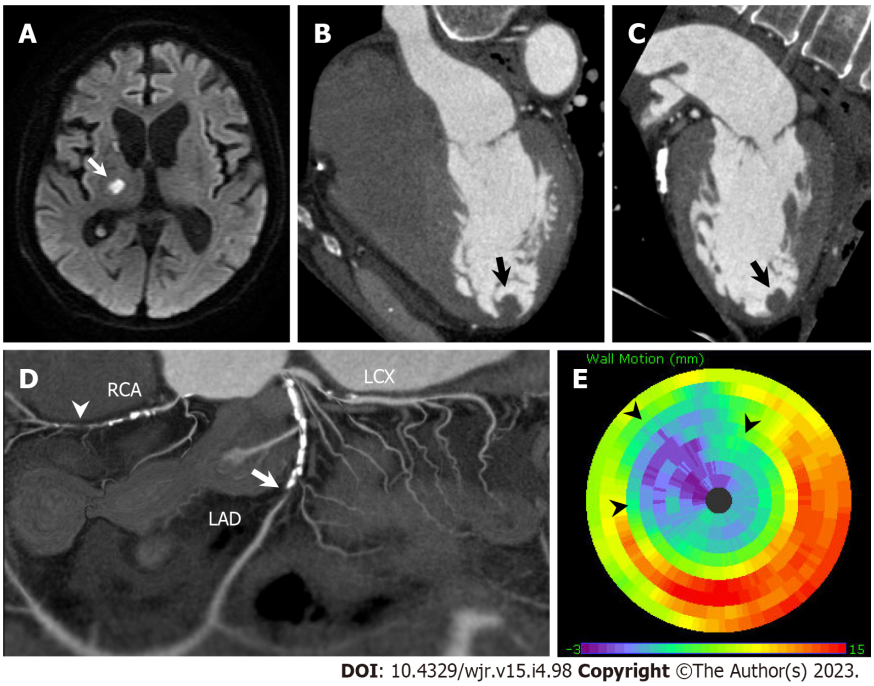

DOI: 10.4329/wjr.v15.i4.98 **Copyright** ©The Author(s) 2023.

Figure 6 Left ventricular thrombus complicated with anteroseptal myocardial infarction. An 80-year-old man hospitalized with acute ischemic stroke underwent cardiac computed tomography (CCT) to rule out obstructive coronary artery disease. A: Diffusion-weighted brain magnetic resonance imaging shows hyperintense lesions in right thalamus and right posterior limb of internal capsule (arrow); B and C: Horizontal long axis (B) and vertical long axis (C) reformatted CCT images show round-shaped thrombus in left ventricular apex (arrow); D: Soap-bubble maximum intensity projection reconstruction image of whole coronary artery shows total occlusion of left anterior descending coronary artery (LAD, arrow) and right coronary artery (RCA, arrowhead); E: Polar map of left ventricular wall motion shows severely reduced anterior to anteroseptal wall motion perfused by LAD (arrowheads). LCX: left circumflex coronary artery.

those with serious clinical manifestations, immediate surgical tumor resection should be performed to prevent devastating embolic complications or sudden cardiac death. While echocardiography remains the first-line imaging modality, CCT has come to be increasingly utilized as a modality for assessing cardiac tumors, particularly when other imaging modalities are non-diagnostic (Figure 11)[8].

Valvular abnormalities

Various valvular abnormalities can lead to thromboembolism, such as infective or noninfective vegetations, and valvular thrombi with or without pannus formation and calcific debris. Several specific valvular abnormalities have been associated with cardioembolic stroke, including infective endocarditis (IE), nonbacterial thrombotic endocarditis, valvular papillary fibroelastoma, biologic or prosthetic valve thrombosis, and valvular calcifications.

Figure 12 shows a case of IE complicated with ischemic stroke. IE is a systemic septic disease that accompanies generation of vegetation containing aggregations of bacteria occurring on the valve, endocardium, and intima of large vessels. Various clinical symptoms are demonstrated in IE, including

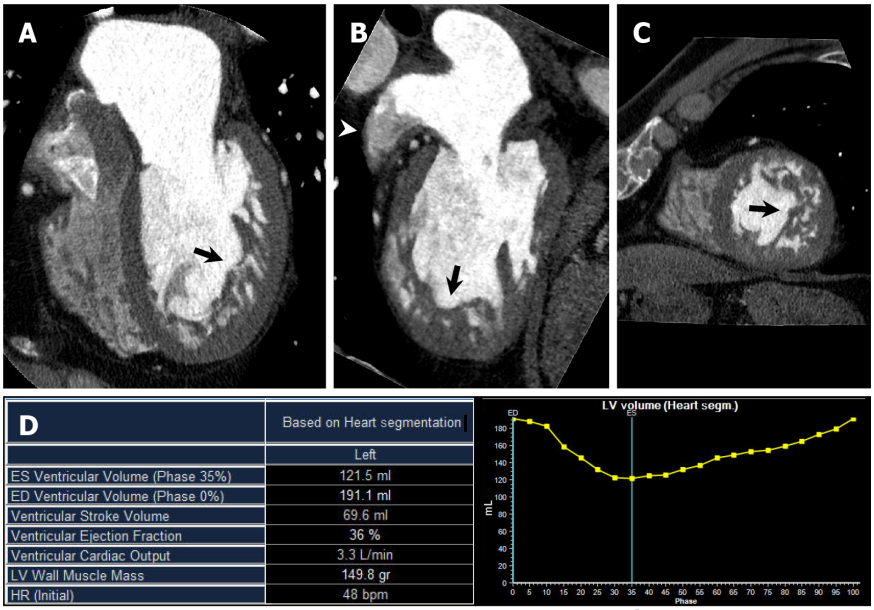

DOI: 10.4329/wjr.v15.i4.98 **Copyright** ©The Author(s) 2023.

Figure 7 Left ventricular noncompaction. A 60-year-old man with congestive heart failure underwent cardiac computed tomography (CCT) in search of underlying heart disease. A–C Horizontal long axis (A), vertical long axis (B), and short axis (C) reformatted CCT images show increased trabeculations from mid to apical portion of left ventricle (arrows). Noncompacted-to-compacted layer ratio at end-diastolic was 2.6. Note contrast heterogeneity within left atrial appendage (LAA), which reflects blood stasis in LAA (arrowhead); D: Left ventricular (LV) functional analysis shows impaired LV function. LV end-diastolic volume, end-systolic volume, and ejection fraction were 191.1 mL, 121.5 mL, and 36%, respectively.

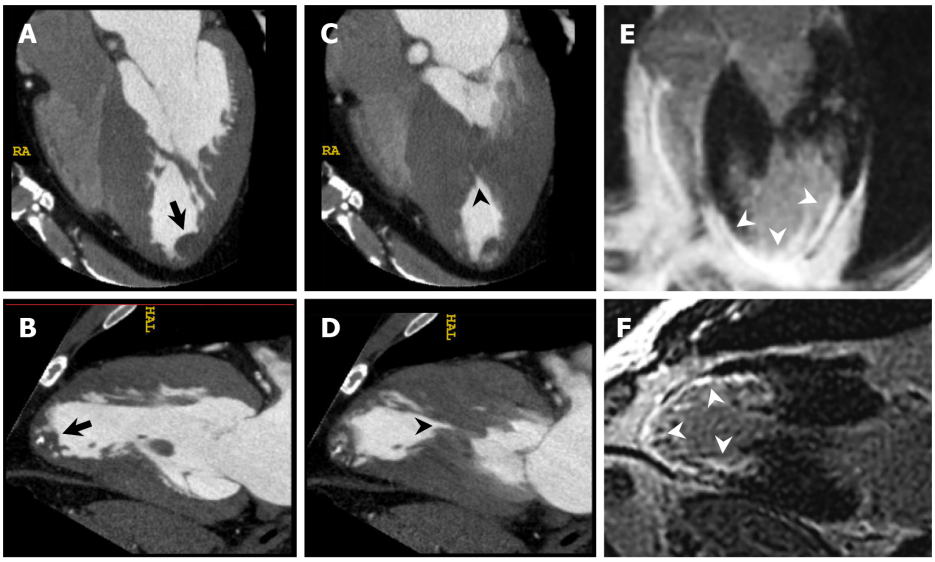

DOI: 10.4329/wjr.v15.i4.98 **Copyright** ©The Author(s) 2023.

Figure 8 Left ventricular apical thrombus complicated with mid-ventricular obstructive hypertrophic cardiomyopathy. A 56-year-old man with unsustained ventricular tachycardia underwent cardiac computed tomography (CCT) in search of underlying heart disease. A and B: Horizontal long axis (A) and vertical long axis (B) reformatted CCT images at end diastole show partially calcified round-shaped thrombus in left ventricular apex (arrow). C and D: Horizontal long axis (C) and vertical long axis (D) reformatted CCT images at end systole show mid-ventricular hypertrophy and mid-cavitary obliteration of left ventricle (arrowhead) with thin-walled left ventricular apical aneurysm; E and F: Horizontal long axis (E) and vertical long axis (F) reformatted images of delayed enhanced cardiac magnetic resonance imaging show transmural late gadolinium enhancement in mid to apical portion of left ventricle (arrowheads).

bacteremia, vascular embolization, and cardiac disorders. Symptomatic neurological complications are seen in 10% to 35% of IE patients, and 65% to 80% of patients show one or more neurological complications when asymptomatic cases are included[39]. Echocardiography is the first-line imaging modality for the diagnosis of IE. TEE is more sensitive than TTE for the detection of both vegetation and periannular complications. However, the sensitivity of echocardiography is lower in IE patients with a prosthetic valve or an intracardiac device, even with the use of TTE. A recent meta-analysis showed that the addition of CCT to TEE can improve diagnostic accuracy for vegetations and periannular complic-

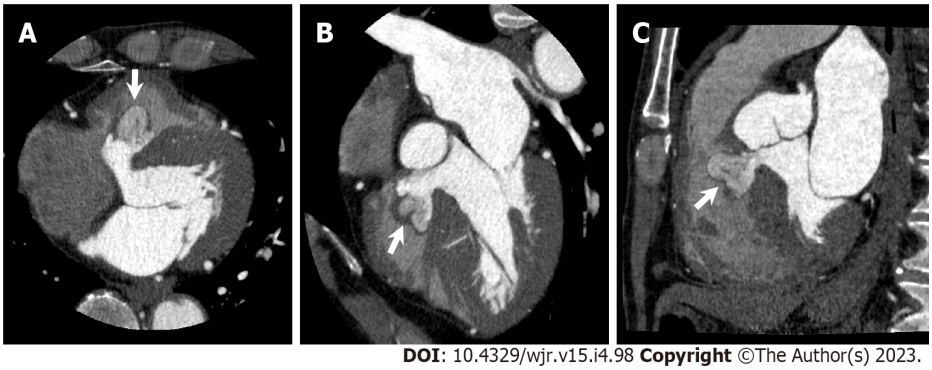

DOI: 10.4329/wjr.v15.i4.98 **Copyright** ©The Author(s) 2023.

Figure 9 Interventricular membranous septal aneurysm. A 78-year-old man underwent cardiac computed tomography (CCT) to further evaluate pathologic outpouching from the left ventricular outflow tract (LVOT) observed on transthoracic echocardiography. A–C: Axial (A), horizontal long axis (B), and sagittal (C) reformatted CCT images show multi-lobular outpouching projecting into right ventricle from LVOT (arrows) consistent with interventricular membranous septal aneurysm (IVMSA), with no evidence of a shunt. Note contrast heterogeneity within IVMSA, which reflects blood stasis in IVMSA.

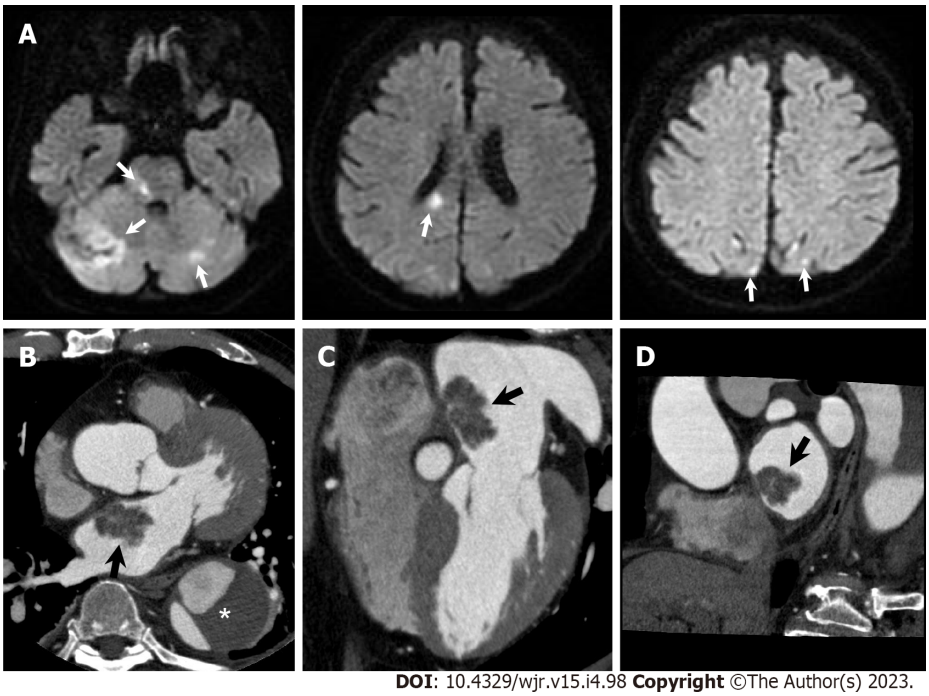

DOI: 10.4329/wjr.v15.i4.98 **Copyright** ©The Author(s) 2023.

Figure 10 Atrial myxoma. A 76-year-old man hospitalized with acute ischemic stroke underwent cardiac computed tomography (CCT) to further evaluate a left atrial mass observed on transthoracic echocardiography. A: Diffusion-weighted brain magnetic resonance imaging shows hyperintense lesions in bilateral cerebellar hemisphere, pons, splenium of corpus callosum, and bilateral occipital lobe (arrows); B–D: Axial (B), horizontal long axis (C), and short axis (D) reformatted CCT images show a 31-mm-sized lobulated left atrial mass attached to the interatrial septum (arrows). He had a previous history of chronic aortic dissection (asterisk). Urgent surgical mass resection was performed. Histological examination confirmed cardiac myxoma.

ations in patients with prosthetic heart valve endocarditis[40].

In patients with prosthetic heart valves, the incidence of thromboembolism ranges from 0.6% to 2.3% per patient-year[41]. The absolute risk of thromboembolism is higher for prosthetic valves in the mitral position than the aortic position. Figure 13 shows a case of mechanical mitral valve dysfunction. The most common causes of prosthetic valve dysfunction are thrombus formation and pannus overgrowth. One particular advantage of CCT is the ability to evaluate patients with mechanical valves, because mechanical valves often have significant artifacts on echocardiography. In the absence of contrast medium administration, CCT can demonstrate abnormal leaflet or disc motion of a mechanical prosthetic valve. Indeed, the opening and closing angles measured by non-contrast CCT strongly correlate with those measured by cinefluoroscopy[42]. In daily clinical practice, doppler-echocardiography is the method of choice to evaluate prosthetic valve function. To identify thrombus or pannus by CCT, contrast enhancement of the blood pool is necessary. Because contrast-enhanced CCT can visualize details of soft-tissue anatomy surrounding the prosthesis, it can provide reliable information for the diagnosis and differentiation of valvular thrombosis and pannus overgrowth when there is suspicion of prosthetic valve dysfunction[43,44].

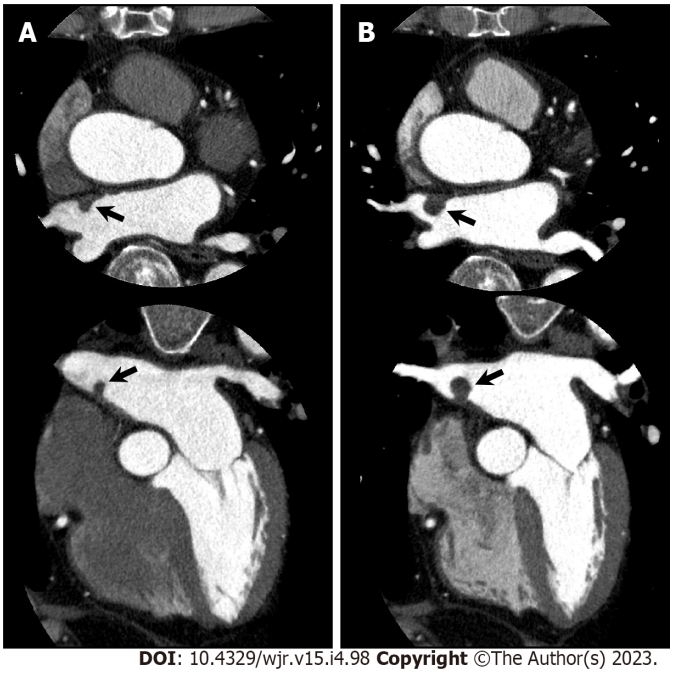

DOI: 10.4329/wjr.v15.i4.98 **Copyright** ©The Author(s) 2023.

Figure 11 Gradually increased atrial myxoma. An 80-year-old man with chest pain underwent cardiac computed tomography (CCT) to evaluate obstructive coronary artery disease. CCT showed severe stenosis in the left anterior descending coronary artery, and percutaneous coronary intervention was performed. Simultaneously, CCT incidentally demonstrated a left atrial mass that could not be visualized on transthoracic echocardiography. A: Axial (upper) and horizontal long axis (lower) reformatted CCT images show left atrial mass of 7 mm by 5 mm in diameter attached to interatrial septum (arrows); B: Axial (upper) and horizontal long axis (lower) reformatted CCT images performed one year later show increased mass size of 11 mm by 11 mm in diameter. Subsequently, elective surgical mass resection was performed. Histological examination confirmed cardiac myxoma.

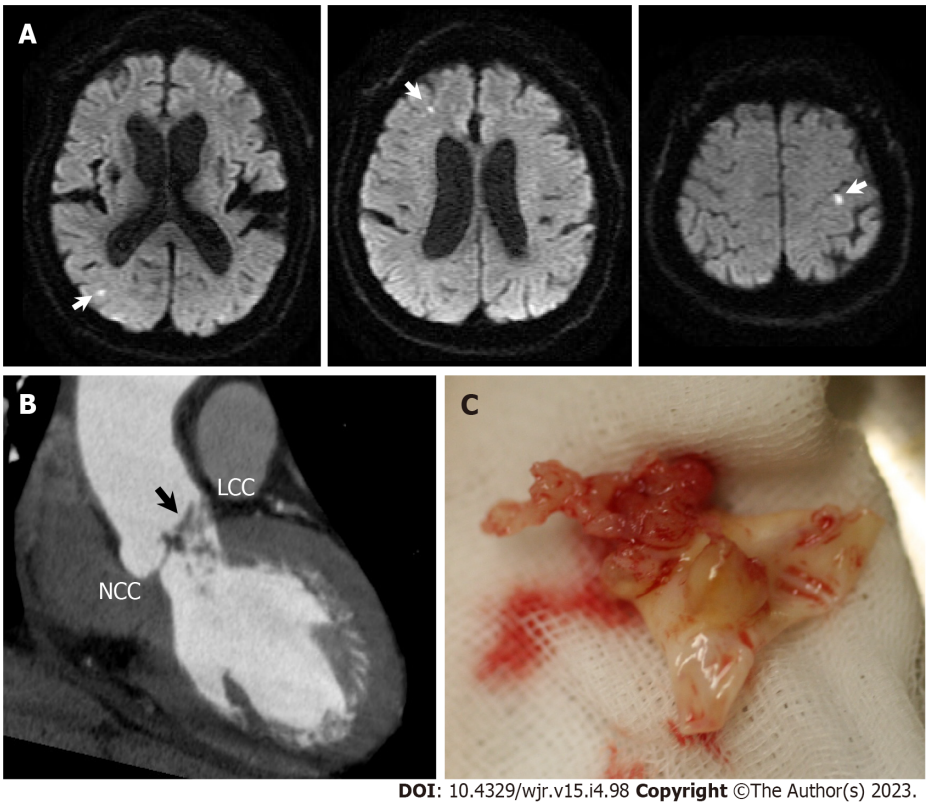

DOI: 10.4329/wjr.v15.i4.98 **Copyright** ©The Author(s) 2023.

Figure 12 Infective endocarditis. A 73-year-old man hospitalized with infective endocarditis and acute ischemic stroke underwent cardiac computed tomography (CCT) to rule out obstructive coronary artery disease before urgent surgical aortic valve replacement. A: Diffusion-weighted brain magnetic resonance imaging shows hyperintense lesions in bilateral cerebral hemisphere (arrows). B: Left ventricular outflow tract long axis reformatted CCT image shows irregularly shaped aortic valve vegetations adherent to left coronary cusp (LCC); C: Surgically resected LCC of aortic valve with fragile vegetations. NCC: Noncoronary cusp.

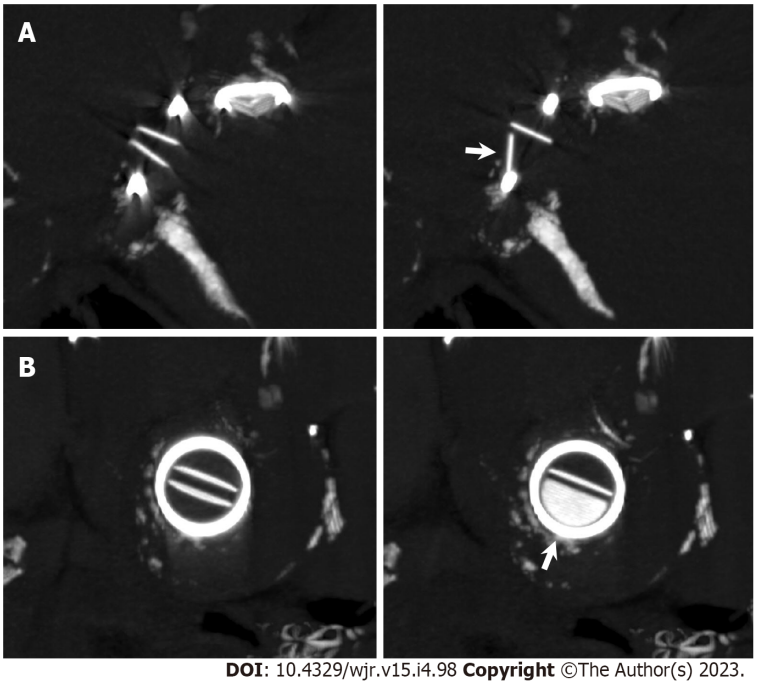

DOI: 10.4329/wjr.v15.i4.98 **Copyright** ©The Author(s) 2023.

Figure 13 Mechanical mitral valve dysfunction. An 86-year-old woman who had undergone St. Jude Medical 29 mm-sized mitral valve replacement 17 years earlier and now presented with congestive heart failure underwent non-contrast cardiac computed tomography (CCT) to evaluate the etiology of mitral regurgitation observed on transthoracic echocardiography. A and B: Multiplanar reformatted images perpendicular to valve leaflet (A) and short axis images (B) of non-contrast CCT show incomplete opening of bileaflet mechanical mitral valve (arrows).

Aortic valve sclerosis and mitral annular calcification are associated with atherosclerotic vascular disease. While their association with stroke reflects their status as a marker for atherosclerotic disease, several reports show their potential as a direct source of calcific or thrombotic debris. Aortic valve sclerosis is irregular thickening and/or calcification of the aortic valve leaflets without significant flow obstruction. The prevalence of aortic valve sclerosis without stenosis increases with age and ranges from 9% in populations with a mean age of 54 to 42% in populations with a mean age of 81. The rate of progression from aortic sclerosis to stenosis is 1.8% to 1.9% per year[45]. Figure 14 shows a case of aortic stenosis (AS) for which evaluation by CCT over time was possible. The coronary artery calcium score is usually calculated by the Agatston method and is a marker of coronary atherosclerotic plaque burden [46]. The severity of aortic sclerosis can also be determined by calculating the Agatston calcium score of the aortic valve. The aortic valve calcium score (AVCS) can help in the classification of AS severity. Reported mean AVCSs were 3219 for severe AS, 1808 for moderate AS, and 584 for mild AS[47]. AVCS is reported to be a useful prognostic imaging marker in AS and is associated with higher rates of mortality during follow-up, with a hazard ratio of 2.11 as a binary threshold[47]. In addition, a higher AVCS is reported to be an independent risk factor for acute stroke after transcatheter aortic valve replacement[48].

Mitral annular calcification (MAC) is defined as calcific deposition in the mitral annulus. Similar to AVCS, the severity of MAC can be determined by calculating the Agatston calcium score. It has been shown that a higher MAC calcium score is associated with increased risk of ischemic stroke[49]. Figure 15 shows a case of caseous MAC. Caseous MAC is a rare variant of MAC with a central liquefaction necrosis that typically affects the posterior annulus. It is sometimes misdiagnosed as a cardiac tumor or abscess. Macroscopically, the inner fluid of the caseous MAC appears as a toothpaste-like milky caseous material. Histological examination of the inner fluid reveals amorphous, eosinophilic acellular content surrounded by macrophages and lymphocytes[50]. A recent comprehensive review of the literature showed that the prevalence of cardioembolic events is significantly higher in patients with caseous MAC than in patients with non-caseous MAC[51]. The high incidence of cardioembolic events in caseous MAC is assumed to be due to spontaneous fistulization and embolization of caseous necrotic debris.

Paradoxical embolism

Paradoxical embolism is a type of stroke or arterial thrombosis caused by embolic sources of venous origin transiting from the right chambers of the heart to the left chambers without passing through the lung filters. Paradoxical embolism can occur *via* interatrial, interventricular, or pulmonary arteriovenous malformations.

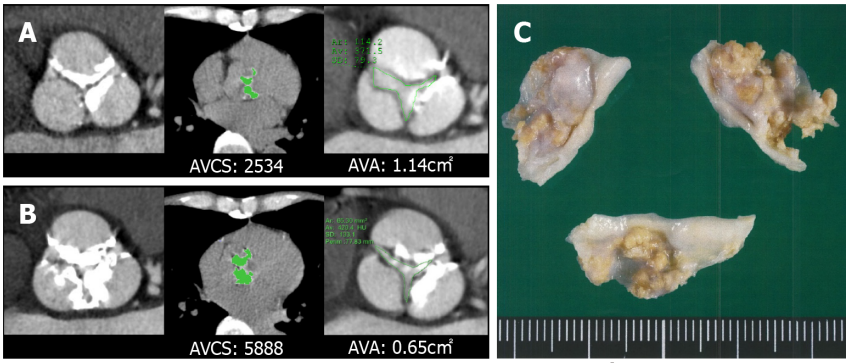

DOI: 10.4329/wjr.v15.i4.98 **Copyright** ©The Author(s) 2023.

Figure 14 Aortic stenosis. A man in his seventies with chronic renal failure requiring hemodialysis and aortic stenosis underwent cardiac computed tomography (CCT) on two occasions to evaluate obstructive coronary artery disease. A: 19 years after initiation of hemodialysis. Left: Short axis reformatted CCT image in diastole shows tricuspid aortic valve with calcification. Middle: Aortic valve calcium score (AVCS) by Agatston method and aortic valve calcium volume were 2534 and 1988 mm^3, respectively. Right: Quantification of aortic valve area (AVA) by planimetry is 1.14 cm^2; B: 24 years after initiation of hemodialysis. Left: Extent of aortic valve calcification has increased. Middle: AVCS by Agatston method and aortic valve calcium volume were 5888 and 4447 mm^3, respectively. Right: Quantification of AVA by planimetry is 0.65 cm^2; C: Surgical aortic valve replacement was performed after second CCT examination. Gross specimen of surgically resected aortic valve is shown.

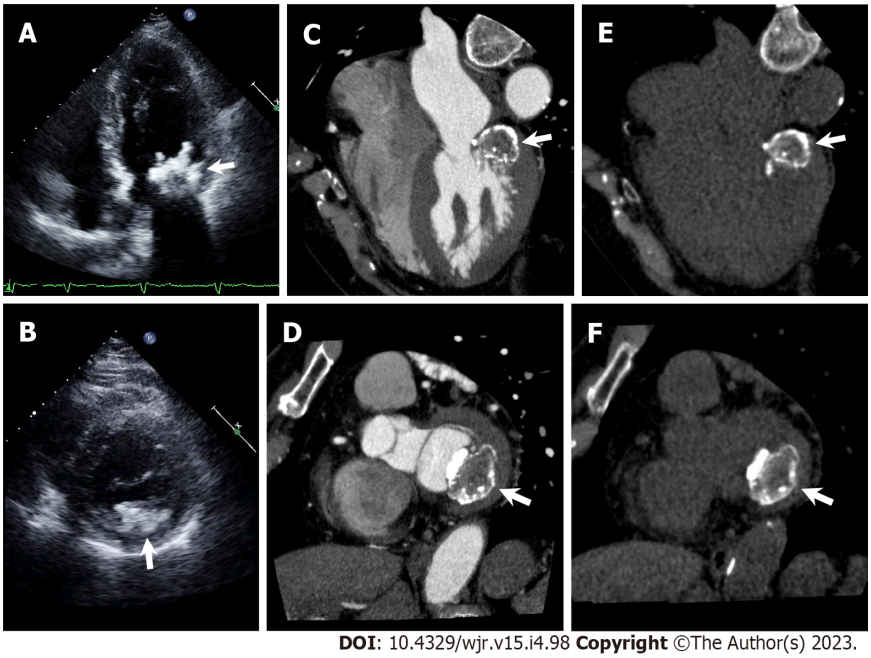

DOI: 10.4329/wjr.v15.i4.98 **Copyright** ©The Author(s) 2023.

Figure 15 Caseous mitral annular calcification. A and B: Apical four chamber view (A) and parasternal short axis view (B) of transthoracic echocardiography show irregularly shaped calcific mass attached to mitral annulus adjacent to posterior mitral valve leaflet (arrows); C–F: Cardiac computed tomography (CCT) images with (C, D) and without (E, F) contrast medium. Horizontal long axis (C, E) and short axis (D, F) reformatted CCT images show a centrally hypodense mass with irregular calcified borders attached to mitral annulus adjacent to posterior mitral valve leaflet (arrows).

A patent foramen ovale (PFO) is an integral part of normal fetal circulation. Although PFOs typically close shortly after birth, they may still be open in approximately 25% to 30% of the general population [52]. Therefore, PFOs are considered to be a normal variant rather than a pathologic finding. By cardiac imaging, a PFO is demonstrated as a flap-like opening at the fossa ovalis, which allows intermittent bidirectional shunting between the atria. A left-to-right shunt is more frequent than a right-to-left shunt. In CCT, a contrast material jet with a flap-like appearance of the interatrial septum is a highly confirmative finding of PFO (Figure 16). In a study of 152 patients with ischemic stroke, both findings of interatrial septum (contrast material jet and flap-like appearance) on CCT yielded sensitivity, specificity, positive predictive value, and negative predictive value of 73.1%, 98.4%, 90.5%, and 94.7%, respectively, compared with TEE as a reference standard[53].

Atrial septal aneurysm (ASA) is a localized sacculation or deformity in the interatrial septum at the level of the fossa ovalis, and protrudes to the right or left atrium or both atria. ASAs are roughly classified into three types according to the direction and movement of protrusion during the cardiac

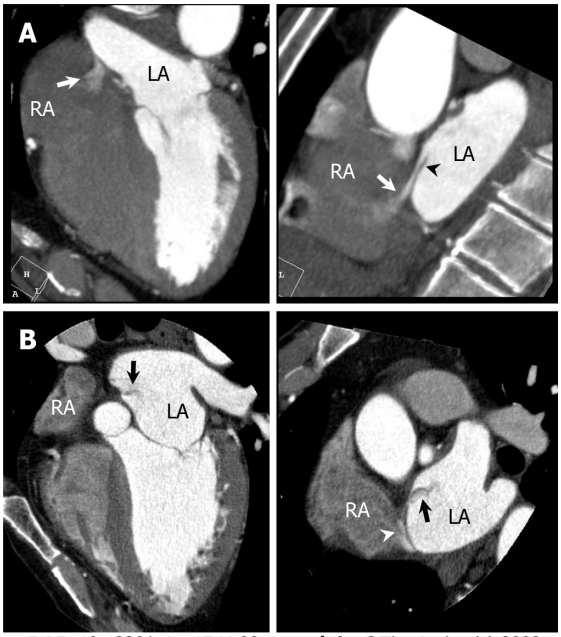

DOI: 10.4329/wjr.v15.i4.98 **Copyright** ©The Author(s) 2023.

Figure 16 Patent foramen ovale. A: Horizontal long axis (left) and short axis oblique (right) reformatted cardiac computed tomography (CCT) images show passage of higher-contrast jet (arrow) from left atrium (LA) *via* patent foramen ovale (PFO) with channel-like appearance (arrowhead) into adjacent right atrium (RA). B: Horizontal long axis (left) and short axis oblique (right) reformatted CCT images show passage of lower-contrast jet (arrow) from RA *via* PFO with channel-like appearance (arrowhead) into adjacent LA.

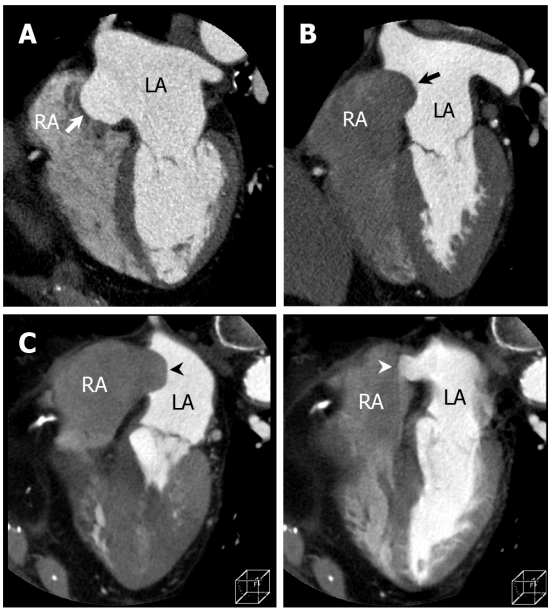

DOI: 10.4329/wjr.v15.i4.98 **Copyright** ©The Author(s) 2023.

Figure 17 Classification of atrial septal aneurysm. A: Cardiac computed tomography (CCT) image of right bulging atrial septal aneurysm [Atrial septal aneurysm (ASA), arrow] in which bulging during cardiac cycle is right atrium (RA) only; B: CCT image of left bulging ASA (arrow) in which bulging during cardiac cycle is left atrium (LA) only; C: CCT image of bidirectional ASA (arrowheads) in which ASA movement during cardiac cycle is bidirectional.

cycle: right-bulging ASA, left-bulging ASA, and bidirectional ASA (Figure 17)[54]. In a study of 103 autopsy hearts, Kuramoto *et al*[55] reported that PFO was more frequently found in subjects with ASA than in those without ASA. A prospective study of 581 patients with cryptogenic stroke showed that a PFO with concomitant ASA is associated with a significant risk of recurrent stroke (Figure 18)[56].

Atrial septal defect (ASD) is the most common congenital heart disease in adults. ASD can also appear in conjunction with ASA (Figure 19). In ASD, CCT shows different features compared with PFO, namely a contrast material jet passing through a sharply defined defect hole, not a channel, in the atrial septum, and perpendicular to the atrial septum. Patients with ASD and right-to-left shunt are at risk for stroke due to paradoxical embolism. ASD is classified in three main types: ostium secundum, ostium

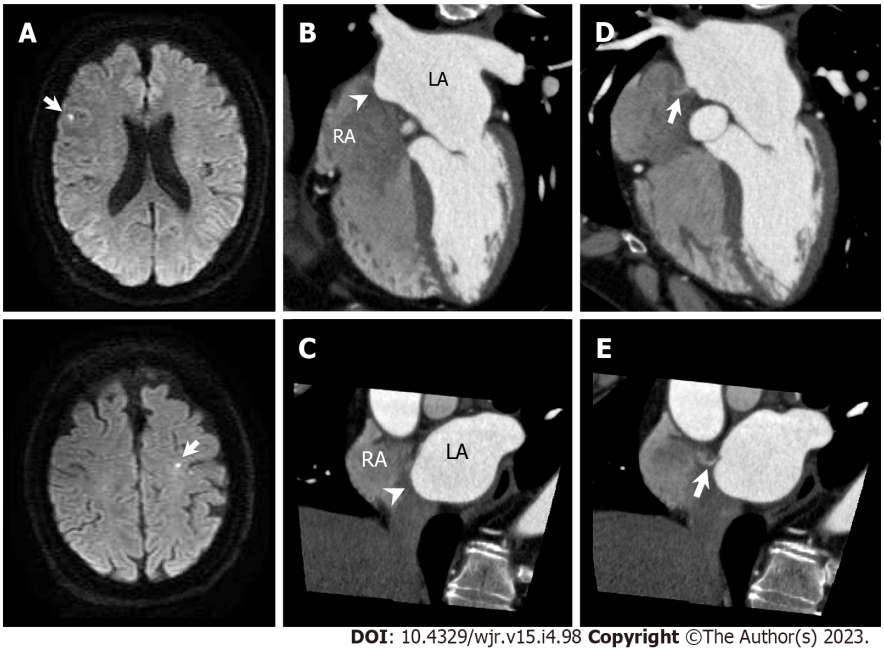

Figure 18 Atrial septal aneurysm with patent foramen ovale. A 53-year-old man with acute ischemic stroke underwent cardiac computed tomography (CCT) to rule out obstructive coronary artery disease. A: Diffusion-weighted brain magnetic resonance imaging shows hyperintense lesions in right frontal lobe and left precentral gyrus (arrows); B and C: Horizontal long axis (B) and short axis oblique (C) reformatted cardiac computed tomography (CCT) images show right bulging atrial septal aneurysm (arrowheads); D and E: Horizontal long axis (D) and short axis oblique (E) reformatted CCT images show small pinhole-like jet from LA *via* patent foramen ovale into RA (arrows). LA: Left atrium; RA: Right atrium.

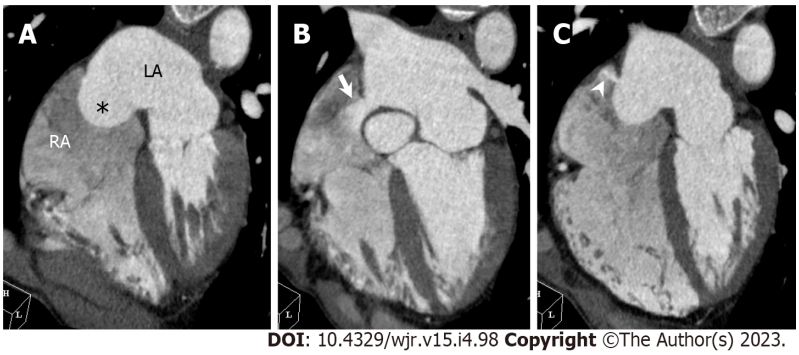

Figure 19 Atrial septal aneurysm with atrial septal defect. A 66-year-old man underwent cardiac computed tomography (CCT) to further evaluate outpouching of the interatrial septum observed on transthoracic echocardiography. Transthoracic echocardiography did not detect interatrial shunt flow. A: Horizontal long axis reformatted CCT image shows right bulging atrial septal aneurysm [Atrial septal aneurysm (ASA), asterisk]. B: Above ASA, in upper portion of interatrial septum just below aortic valve, atrial septal defect (ASD) with contrast shunt from LA into RA is found (arrow). Measured size of ASD is 14 mm by 10 mm; C: Below ASA, in lower portion of interatrial septum, another 5 mm-sized ASD with left to right shunt is found (arrowhead). LA: Left atrium; RA: Right atrium.

primum, and sinus venosus. Coronary sinus ASD is very rare. Echocardiography is generally an accurate means in the diagnosis of most secundum and primum ASDs, but sinus venosus ASDs are sometimes overlooked. CCT is a useful supplementary imaging modality for depicting sinus venosus ASDs and defining associated partial anomalous pulmonary venous return (Figure 20)[57].

Pulmonary arteriovenous malformations are structurally abnormal vessels that provide direct communication between a pulmonary artery and vein, and the absence of lung filtering capillary beds offers the potential for paradoxical embolism[58]. CT is recognized to be the gold standard investigation for diagnosis and also plays an important role in treatment planning. They are demonstrated as a nodule or serpiginous mass connected with blood vessels (Figure 21).

CONCLUSION

CCT can provide high-quality information about the causal heart disease in patients with cardioembolic stroke. In addition, CCT can simultaneously evaluate obstructive coronary artery disease, which may be

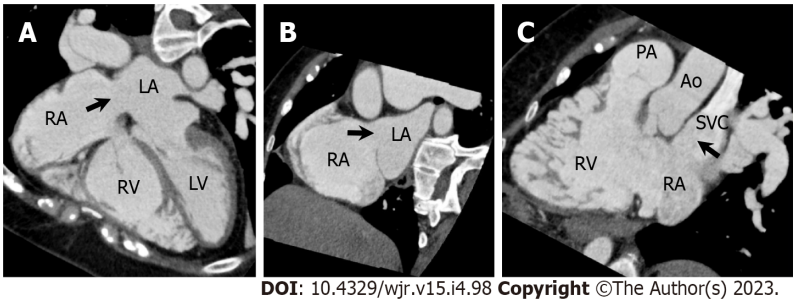

DOI: 10.4329/wjr.v15.i4.98 **Copyright** ©The Author(s) 2023.

Figure 20 Superior sinus venosus atrial septal defect. A 57-year-old woman underwent cardiac computed tomography (CCT) to evaluate right ventricular (RV) morphology and function because transthoracic echocardiography revealed gradual RV dilatation over time. She had a previous history of cryptogenic ischemic stroke when she was 3 years old. A–C: Horizontal long axis (A), short axis oblique (B), and RV long axis reformatted CCT images show atrial septal defect (ASD) in superior aspect of interatrial septum at level of entry of superior vena cava (SVC, arrows). Measured size of ASD is 26 mm by 25 mm. Partial anomalous pulmonary venous return is not complicated. Subsequently, she underwent right and left heart catheterization. The Qp/Qs ratio and mean pulmonary artery pressure measured using right heart catheterization were 4.8 and 23 mmHg, respectively. Surgical ASD closure was performed. LA: Left atrium; LV: Left ventricle; RA: Right atrium; PA: Pulmonary artery; Ao: Aorta.

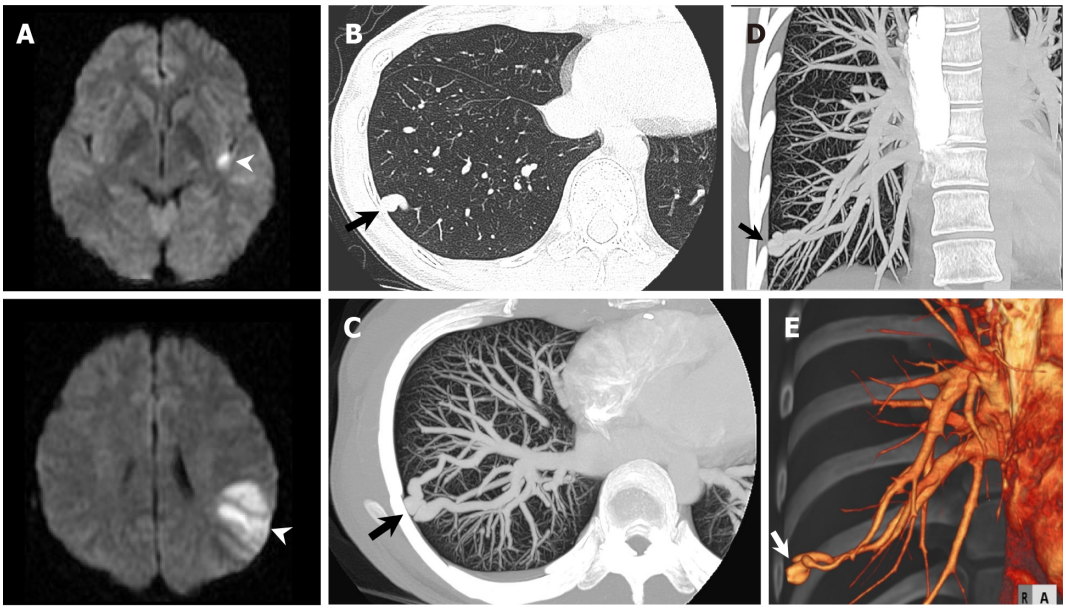

DOI: 10.4329/wjr.v15.i4.98 **Copyright** ©The Author(s) 2023.

Figure 21 Pulmonary arteriovenous malformation. A 31-year-old woman hospitalized with acute ischemic stroke underwent chest computed tomography (CT) to further evaluate a nodular shadow in right lower lung field on chest radiography. A: Diffusion-weighted brain magnetic resonance imaging shows hyperintense lesions in left insula and left parietal lobe (arrowheads); B: Non-contrast chest CT shows nodular shadow in lateral basal segment of right inferior lobe (arrow); C–E: Maximum intensity projection reconstruction images (C: Axial; D: Coronal) and three-dimensional volume-rendered image (E) of contrast-enhanced CT show pulmonary arteriovenous malformation in lateral basal segment of right inferior lobe (arrow).

helpful in surgical planning in patients who need urgent surgery, such as for cardiac myxoma or infective endocarditis. However, clinicians should sift through the information derived from CCT and determine whether the clinical symptoms, physical findings, and results of neuroimaging are consistent with the causal relationship in individual patients with ischemic stroke.

FOOTNOTES

Author contributions: Yoshihara S made all of this manuscript and figures.

Conflict-of-interest statement: Shu Yoshihara does not have any conflict-of-interest.

Country/Territory of origin: Japan

ORCID number: Shu Yoshihara 0000-0001-9294-3767.

S-Editor: Liu JH
L-Editor: A
P-Editor: Zhao S

REFERENCES

1 **Adams HP Jr**, Bendixen BH, Kappelle LJ, Biller J, Love BB, Gordon DL, Marsh EE 3rd. Classification of subtype of acute ischemic stroke. Definitions for use in a multicenter clinical trial. TOAST. Trial of Org 10172 in Acute Stroke Treatment. *Stroke* 1993; **24**: 35-41 [PMID: 7678184 DOI: 10.1161/01.str.24.1.35]

2 **Amarenco P**, Bogousslavsky J, Caplan LR, Donnan GA, Hennerici MG. New approach to stroke subtyping: the A-S-C-O (phenotypic) classification of stroke. *Cerebrovasc Dis* 2009; **27**: 502-508 [PMID: 19342826 DOI: 10.1159/000210433]

3 **Powers WJ**, Rabinstein AA, Ackerson T, Adeoye OM, Bambakidis NC, Becker K, Biller J, Brown M, Demaerschalk BM, Hoh B, Jauch EC, Kidwell CS, Leslie-Mazwi TM, Ovbiagele B, Scott PA, Sheth KN, Southerland AM, Summers DV, Tirschwell DL. Guidelines for the Early Management of Patients With Acute Ischemic Stroke: 2019 Update to the 2018 Guidelines for the Early Management of Acute Ischemic Stroke: A Guideline for Healthcare Professionals From the American Heart Association/American Stroke Association. *Stroke* 2019; **50**: e344-e418 [PMID: 31662037 DOI: 10.1161/STR.0000000000000211]

4 **de Bruijn SF**, Agema WR, Lammers GJ, van der Wall EE, Wolterbeek R, Holman ER, Bollen EL, Bax JJ. Transesophageal echocardiography is superior to transthoracic echocardiography in management of patients of any age with transient ischemic attack or stroke. *Stroke* 2006; **37**: 2531-2534 [PMID: 16946152 DOI: 10.1161/01.STR.0000241064.46659.69]

5 **Strandberg M**, Marttila RJ, Helenius H, Hartiala J. Transoesophageal echocardiography in selecting patients for anticoagulation after ischaemic stroke or transient ischaemic attack. *J Neurol Neurosurg Psychiatry* 2002; **73**: 29-33 [PMID: 12082041 DOI: 10.1136/jnnp.73.1.29]

6 **Knuuti J**, Ballo H, Juarez-Orozco LE, Saraste A, Kolh P, Rutjes AWS, Jüni P, Windecker S, Bax JJ, Wijns W. The performance of non-invasive tests to rule-in and rule-out significant coronary artery stenosis in patients with stable angina: a meta-analysis focused on post-test disease probability. *Eur Heart J* 2018; **39**: 3322-3330 [PMID: 29850808 DOI: 10.1093/eurheartj/ehy267]

7 **Leipsic J**, Abbara S, Achenbach S, Cury R, Earls JP, Mancini GJ, Nieman K, Pontone G, Raff GL. SCCT guidelines for the interpretation and reporting of coronary CT angiography: a report of the Society of Cardiovascular Computed Tomography Guidelines Committee. *J Cardiovasc Comput Tomogr* 2014; **8**: 342-358 [PMID: 25301040 DOI: 10.1016/j.jcct.2014.07.003]

8 **Taylor AJ**, Cerqueira M, Hodgson JM, Mark D, Min J, O'Gara P, Rubin GD; American College of Cardiology Foundation Appropriate Use Criteria Task Force; Society of Cardiovascular Computed Tomography; American College of Radiology; American Heart Association; American Society of Echocardiography; American Society of Nuclear Cardiology; North American Society for Cardiovascular Imaging; Society for Cardiovascular Angiography and Interventions; Society for Cardiovascular Magnetic Resonance. ACCF/SCCT/ACR/AHA/ASE/ASNC/NASCI/SCAI/SCMR 2010 Appropriate Use Criteria for Cardiac Computed Tomography. A Report of the American College of Cardiology Foundation Appropriate Use Criteria Task Force, the Society of Cardiovascular Computed Tomography, the American College of Radiology, the American Heart Association, the American Society of Echocardiography, the American Society of Nuclear Cardiology, the North American Society for Cardiovascular Imaging, the Society for Cardiovascular Angiography and Interventions, and the Society for Cardiovascular Magnetic Resonance. *J Cardiovasc Comput Tomogr* 2010; **4**: 407.e1-407.33 [PMID: 21232696 DOI: 10.1016/j.jcct.2010.11.001]

9 **Lupercio F**, Carlos Ruiz J, Briceno DF, Romero J, Villablanca PA, Berardi C, Faillace R, Krumerman A, Fisher JD, Ferrick K, Garcia M, Natale A, Di Biase L. Left atrial appendage morphology assessment for risk stratification of embolic stroke in patients with atrial fibrillation: A meta-analysis. *Heart Rhythm* 2016; **13**: 1402-1409 [PMID: 27016474 DOI: 10.1016/j.hrthm.2016.03.042]

10 **Kim YY**, Klein AL, Halliburton SS, Popovic ZB, Kuzmiak SA, Sola S, Garcia MJ, Schoenhagen P, Natale A, Desai MY. Left atrial appendage filling defects identified by multidetector computed tomography in patients undergoing radiofrequency pulmonary vein antral isolation: a comparison with transesophageal echocardiography. *Am Heart J* 2007; **154**: 1199-1205 [PMID: 18035095 DOI: 10.1016/j.ahj.2007.08.004]

11 **Kim SC**, Chun EJ, Choi SI, Lee SJ, Chang HJ, Han MK, Bae HJ, Park JH. Differentiation between spontaneous echocardiographic contrast and left atrial appendage thrombus in patients with suspected embolic stroke using two-phase multidetector computed tomography. *Am J Cardiol* 2010; **106**: 1174-1181 [PMID: 20920660 DOI: 10.1016/j.amjcard.2010.06.033]

12 **Hsieh BP**, Jha O, Chandra R, Garcia M, Boxt L, Taub C. Novel computed tomography indexes of left atrial appendage stasis. *Int J Cardiovasc Imaging* 2013; **29**: 237-244 [PMID: 22588712 DOI: 10.1007/s10554-012-0062-0]

13 **Kawaji T**, Yamgami S, Shizuta S, Aizawa T, Kato M, Yokomatsu T, Miki S, Ono K, Kimura T. Relation of a Filling Defect of Left Atrial Appendage by Contrast Computed Tomography Image With Subsequent Clinical Events in Patients With Atrial Fibrillation Receiving Catheter Ablation Procedures. *Am J Cardiol* 2022; **180**: 29-36 [PMID: 35863941 DOI: 10.1016/j.amjcard.2022.06.009]

14 **Romero J**, Husain SA, Kelesidis I, Sanz J, Medina HM, Garcia MJ. Detection of left atrial appendage thrombus by cardiac computed tomography in patients with atrial fibrillation: a meta-analysis. *Circ Cardiovasc Imaging* 2013; **6**: 185-194 [PMID: 23406625 DOI: 10.1161/CIRCIMAGING.112.000153]

15 **Wolf PA**, Dawber TR, Thomas HE Jr, Kannel WB. Epidemiologic assessment of chronic atrial fibrillation and risk of stroke: the Framingham study. *Neurology* 1978; **28**: 973-977 [PMID: 570666 DOI: 10.1212/wnl.28.10.973]

16 **Salem DN**, Daudelin HD, Levine HJ, Pauker SG, Eckman MH, Riff J. Antithrombotic therapy in valvular heart disease. *Chest* 2001; **119**: 207S-219S [PMID: 11157650 DOI: 10.1378/chest.119.1_suppl.207s]

17 **Somerville W**, Chambers RJ. Systemic embolism in mitral stenosis: relation to the size of the left atrial appendix. *Br Med J* 1964; **2**: 1167-1169 [PMID: 14190485 DOI: 10.1136/bmj.2.5418.1167]

18 **Taina M**, Vanninen R, Hedman M, Jäkälä P, Kärkkäinen S, Tapiola T, Sipola P. Left atrial appendage volume increased in more than half of patients with cryptogenic stroke. *PLoS One* 2013; **8**: e79519 [PMID: 24223960 DOI: 10.1371/journal.pone.0079519]

19 **Veinot JP**, Harrity PJ, Gentile F, Khandheria BK, Bailey KR, Eickholt JT, Seward JB, Tajik AJ, Edwards WD. Anatomy of the normal left atrial appendage: a quantitative study of age-related changes in 500 autopsy hearts: implications for echocardiographic examination. *Circulation* 1997; **96**: 3112-3115 [PMID: 9386182 DOI: 10.1161/01.cir.96.9.3112]

20 **Aryal MR**, Hakim FA, Ghimire S, Giri S, Pandit A, Bhandari Y, Bhandari N, Pathak R, Karmacharya P, Pradhan R. Left atrial appendage aneurysm: a systematic review of 82 cases. *Echocardiography* 2014; **31**: 1312-1318 [PMID: 24976376 DOI: 10.1111/echo.12667]

21 **Boucebci S**, Pambrun T, Velasco S, Duboe PO, Ingrand P, Tasu JP. Assessment of normal left atrial appendage anatomy and function over gender and ages by dynamic cardiac CT. *Eur Radiol* 2016; **26**: 1512-1520 [PMID: 26310584 DOI: 10.1007/s00330-015-3962-2]

22 **Maan A**, Heist EK. Left Atrial Appendage Anatomy: Implications for Endocardial Catheter-based Device Closure. *J Innov Card Rhythm Manag* 2020; **11**: 4179-4186 [PMID: 32724709 DOI: 10.19102/icrm.2020.110704]

23 **Kimura T**, Takatsuki S, Inagawa K, Katsumata Y, Nishiyama T, Nishiyama N, Fukumoto K, Aizawa Y, Tanimoto Y, Tanimoto K, Jinzaki M, Fukuda K. Anatomical characteristics of the left atrial appendage in cardiogenic stroke with low CHADS2 scores. *Heart Rhythm* 2013; **10**: 921-925 [PMID: 23384894 DOI: 10.1016/j.hrthm.2013.01.036]

24 **Asinger RW**, Mikell FL, Elsperger J, Hodges M. Incidence of left-ventricular thrombosis after acute transmural myocardial infarction. Serial evaluation by two-dimensional echocardiography. *N Engl J Med* 1981; **305**: 297-302 [PMID: 7242633 DOI: 10.1056/NEJM198108063050601]

25 **Gianstefani S**, Douiri A, Delithanasis I, Rogers T, Sen A, Kalra S, Charangwa L, Reiken J, Monaghan M, MacCarthy P. Incidence and predictors of early left ventricular thrombus after ST-elevation myocardial infarction in the contemporary era of primary percutaneous coronary intervention. *Am J Cardiol* 2014; **113**: 1111-1116 [PMID: 24485697 DOI: 10.1016/j.amjcard.2013.12.015]

26 **Loh E**, Sutton MS, Wun CC, Rouleau JL, Flaker GC, Gottlieb SS, Lamas GA, Moyé LA, Goldhaber SZ, Pfeffer MA. Ventricular dysfunction and the risk of stroke after myocardial infarction. *N Engl J Med* 1997; **336**: 251-257 [PMID: 8995087 DOI: 10.1056/NEJM199701233360403]

27 **Weinsaft JW**, Kim HW, Shah DJ, Klem I, Crowley AL, Brosnan R, James OG, Patel MR, Heitner J, Parker M, Velazquez EJ, Steenbergen C, Judd RM, Kim RJ. Detection of left ventricular thrombus by delayed-enhancement cardiovascular magnetic resonance prevalence and markers in patients with systolic dysfunction. *J Am Coll Cardiol* 2008; **52**: 148-157 [PMID: 18598895 DOI: 10.1016/j.jacc.2008.03.041]

28 **Grant MD**, Mann RD, Kristenson SD, Buck RM, Mendoza JD, Reese JM, Grant DW, Roberge EA. Transthoracic Echocardiography: Beginner's Guide with Emphasis on Blind Spots as Identified with CT and MRI. *Radiographics* 2021; **41**: 1022-1042 [PMID: 34115535 DOI: 10.1148/rg.2021200142]

29 **Weinsaft JW**, Kim HW, Crowley AL, Klem I, Shenoy C, Van Assche L, Brosnan R, Shah DJ, Velazquez EJ, Parker M, Judd RM, Kim RJ. LV thrombus detection by routine echocardiography: insights into performance characteristics using delayed enhancement CMR. *JACC Cardiovasc Imaging* 2011; **4**: 702-712 [PMID: 21757159 DOI: 10.1016/j.jcmg.2011.03.017]

30 **Ghadri JR**, Wittstein IS, Prasad A, Sharkey S, Dote K, Akashi YJ, Cammann VL, Crea F, Galiuto L, Desmet W, Yoshida T, Manfredini R, Eitel I, Kosuge M, Nef HM, Deshmukh A, Lerman A, Bossone E, Citro R, Ueyama T, Corrado D, Kurisu S, Ruschitzka F, Winchester D, Lyon AR, Omerovic E, Bax JJ, Meimoun P, Tarantini G, Rihal C, Y-Hassan S, Migliore F, Horowitz JD, Shimokawa H, Lüscher TF, Templin C. International Expert Consensus Document on Takotsubo Syndrome (Part II): Diagnostic Workup, Outcome, and Management. *Eur Heart J* 2018; **39**: 2047-2062 [PMID: 29850820 DOI: 10.1093/eurheartj/ehy077]

31 **Freudenberger RS**, Hellkamp AS, Halperin JL, Poole J, Anderson J, Johnson G, Mark DB, Lee KL, Bardy GH; SCD-HeFT Investigators. Risk of thromboembolism in heart failure: an analysis from the Sudden Cardiac Death in Heart Failure Trial (SCD-HeFT). *Circulation* 2007; **115**: 2637-2641 [PMID: 17485579 DOI: 10.1161/CIRCULATIONAHA.106.661397]

32 **McDonagh TA**, Metra M, Adamo M, Gardner RS, Baumbach A, Böhm M, Burri H, Butler J, Čelutkienė J, Chioncel O, Cleland JGF, Coats AJS, Crespo-Leiro MG, Farmakis D, Gilard M, Heymans S, Hoes AW, Jaarsma T, Jankowska EA, Lainscak M, Lam CSP, Lyon AR, McMurray JJV, Mebazaa A, Mindham R, Muneretto C, Francesco Piepoli M, Price S, Rosano GMC, Ruschitzka F, Kathrine Skibelund A; ESC Scientific Document Group. 2021 ESC Guidelines for the diagnosis and treatment of acute and chronic heart failure. *Eur Heart J* 2021; **42**: 3599-3726 [PMID: 34447992 DOI: 10.1093/eurheartj/ehab368]

33 **Cui L**, Tse G, Zhao Z, Bazoukis G, Letsas KP, Korantzopoulos P, Roever L, Li G, Liu T. Mid-ventricular obstructive hypertrophic cardiomyopathy with apical aneurysm: An important subtype of arrhythmogenic cardiomyopathy. *Ann Noninvasive Electrocardiol* 2019; **24**: e12638 [PMID: 30737990 DOI: 10.1111/anec.12638]

34 **Papanastasiou CA**, Zegkos T, Karamitsos TD, Rowin EJ, Maron MS, Parcharidou D, Kokkinidis DG, Karvounis H, Rimoldi O, Maron BJ, Efthimiadis GK. Prognostic role of left ventricular apical aneurysm in hypertrophic cardiomyopathy: A systematic review and meta-analysis. *Int J Cardiol* 2021; **332**: 127-132 [PMID: 33794232 DOI:

10.1016/j.ijcard.2021.03.056]
35 **Carcano C**, Kanne JP, Kirsch J. Interventricular membranous septal aneurysm: CT and MR manifestations. *Insights Imaging* 2016; **7**: 111-117 [PMID: 26687514 DOI: 10.1007/s13244-015-0456-3]
36 **Tyebally S**, Chen D, Bhattacharyya S, Mughrabi A, Hussain Z, Manisty C, Westwood M, Ghosh AK, Guha A. Cardiac Tumors: JACC CardioOncology State-of-the-Art Review. *JACC CardioOncol* 2020; **2**: 293-311 [PMID: 34396236 DOI: 10.1016/j.jaccao.2020.05.009]
37 **Pinede L**, Duhaut P, Loire R. Clinical presentation of left atrial cardiac myxoma. A series of 112 consecutive cases. *Medicine (Baltimore)* 2001; **80**: 159-172 [PMID: 11388092 DOI: 10.1097/00005792-200105000-00002]
38 **Lee VH**, Connolly HM, Brown RD Jr. Central nervous system manifestations of cardiac myxoma. *Arch Neurol* 2007; **64**: 1115-1120 [PMID: 17698701 DOI: 10.1001/archneur.64.8.1115]
39 **Nakatani S**, Ohara T, Ashihara K, Izumi C, Iwanaga S, Eishi K, Okita Y, Daimon M, Kimura T, Toyoda K, Nakase H, Nakano K, Higashi M, Mitsutake K, Murakami T, Yasukochi S, Okazaki S, Sakamoto H, Tanaka H, Nakagawa I, Nomura R, Fujiu K, Miura T, Morizane T; Japanese Circulation Society Joint Working Group. JCS 2017 Guideline on Prevention and Treatment of Infective Endocarditis. *Circ J* 2019; **83**: 1767-1809 [PMID: 31281136 DOI: 10.1253/circj.CJ-19-0549]
40 **Habets J**, Tanis W, Reitsma JB, van den Brink RB, Mali WP, Chamuleau SA, Budde RP. Are novel non-invasive imaging techniques needed in patients with suspected prosthetic heart valve endocarditis? *Eur Radiol* 2015; **25**: 2125-2133 [PMID: 25680715 DOI: 10.1007/s00330-015-3605-7]
41 **Writing Committee Members**, Otto CM, Nishimura RA, Bonow RO, Carabello BA, Erwin JP 3rd, Gentile F, Jneid H, Krieger EV, Mack M, McLeod C, O'Gara PT, Rigolin VH, Sundt TM 3rd, Thompson A, Toly C; ACC/AHA Joint Committee Members, O'Gara PT, Beckman JA, Levine GN, Al-Khatib SM, Armbruster A, Birtcher KK, Ciggaroa J, Deswal A, Dixon DL, Fleisher LA, de Las Fuentes L, Gentile F, Goldberger ZD, Gorenek B, Haynes N, Hernandez AF, Hlatky MA, Joglar JA, Jones WS, Marine JE, Mark D, Palaniappan L, Piano MR, Spatz ES, Tamis-Holland J, Wijeysundera DN, Woo YJ. 2020 ACC/AHA guideline for the management of patients with valvular heart disease: A report of the American College of Cardiology/American Heart Association Joint Committee on Clinical Practice Guidelines. *J Thorac Cardiovasc Surg* 2021; **162**: e183-e353 [PMID: 33972115 DOI: 10.1016/j.jtcvs.2021.04.002]
42 **Bazeed MF**, Moselhy MS, Rezk AI, Al-Murayeh MA. Low radiation dose non-contrast cardiac CT: is it of value in the evaluation of mechanical aortic valve. *Acta Radiol* 2012; **53**: 389-393 [PMID: 22422269 DOI: 10.1258/ar.2012.110253]
43 **Gündüz S**, Özkan M, Kalçik M, Gürsoy OM, Astarcioğlu MA, Karakoyun S, Aykan AÇ, Biteker M, Gökdeniz T, Kaya H, Yesin M, Duran NE, Sevinç D, Güneysu T. Sixty-Four-Section Cardiac Computed Tomography in Mechanical Prosthetic Heart Valve Dysfunction: Thrombus or Pannus. *Circ Cardiovasc Imaging* 2015; **8** [PMID: 26659372 DOI: 10.1161/CIRCIMAGING.115.003246]
44 **Suh YJ**, Lee S, Im DJ, Chang S, Hong YJ, Lee HJ, Hur J, Choi BW, Chang BC, Shim CY, Hong GR, Kim YJ. Added value of cardiac computed tomography for evaluation of mechanical aortic valve: Emphasis on evaluation of pannus with surgical findings as standard reference. *Int J Cardiol* 2016; **214**: 454-460 [PMID: 27096962 DOI: 10.1016/j.ijcard.2016.04.011]
45 **Coffey S**, Cox B, Williams MJ. The prevalence, incidence, progression, and risks of aortic valve sclerosis: a systematic review and meta-analysis. *J Am Coll Cardiol* 2014; **63**: 2852-2861 [PMID: 24814496 DOI: 10.1016/j.jacc.2014.04.018]
46 **Agatston AS**, Janowitz WR, Hildner FJ, Zusmer NR, Viamonte M Jr, Detrano R. Quantification of coronary artery calcium using ultrafast computed tomography. *J Am Coll Cardiol* 1990; **15**: 827-832 [PMID: 2407762 DOI: 10.1016/0735-1097(90)90282-t]
47 **Wang TKM**, Flamm SD, Schoenhagen P, Griffin BP, Rodriguez LL, Grimm RA, Xu B. Diagnostic and Prognostic Performance of Aortic Valve Calcium Score with Cardiac CT for Aortic Stenosis: A Meta-Analysis. *Radiol Cardiothorac Imaging* 2021; **3**: e210075 [PMID: 34498008 DOI: 10.1148/ryct.2021210075]
48 **Foley M**, Hall K, Howard JP, Ahmad Y, Gandhi M, Mahboobani S, Okafor J, Rahman H, Hadjiloizou N, Ruparelia N, Mikhail G, Malik I, Kanaganayagam G, Sutaria N, Rana B, Ariff B, Barden E, Anderson J, Afoke J, Petraco R, Al-Lamee R, Sen S. Aortic Valve Calcium Score Is Associated With Acute Stroke in Transcatheter Aortic Valve Replacement Patients. *J Soc Cardiovasc Angiogr Interv* 2022; **1**: 100349 [PMID: 35992189 DOI: 10.1016/j.jscai.2022.100349]
49 **Kianoush S**, Al Rifai M, Cainzos-Achirica M, Al-Mallah MH, Tison GH, Yeboah J, Miedema MD, Allison MA, Wong ND, DeFilippis AP, Longstreth W, Nasir K, Budoff MJ, Matsushita K, Blaha MJ. Thoracic extra-coronary calcification for the prediction of stroke: The Multi-Ethnic Study of Atherosclerosis. *Atherosclerosis* 2017; **267**: 61-67 [PMID: 29100062 DOI: 10.1016/j.atherosclerosis.2017.10.010]
50 **Harpaz D**, Auerbach I, Vered Z, Motro M, Tobar A, Rosenblatt S. Caseous calcification of the mitral annulus: a neglected, unrecognized diagnosis. *J Am Soc Echocardiogr* 2001; **14**: 825-831 [PMID: 11490332 DOI: 10.1067/mje.2001.111877]
51 **Dietl CA**, Hawthorn CM, Raizada V. Risk of Cerebral Embolization with Caseous Calcification of the Mitral Annulus: Review Article. *Open Cardiovasc Med J* 2016; **10**: 221-232 [PMID: 27990181 DOI: 10.2174/1874192401610010221]
52 **Hagen PT**, Scholz DG, Edwards WD. Incidence and size of patent foramen ovale during the first 10 decades of life: an autopsy study of 965 normal hearts. *Mayo Clin Proc* 1984; **59**: 17-20 [PMID: 6694427 DOI: 10.1016/s0025-6196(12)60336-x]
53 **Kim YJ**, Hur J, Shim CY, Lee HJ, Ha JW, Choe KO, Heo JH, Choi EY, Choi BW. Patent foramen ovale: diagnosis with multidetector CT--comparison with transesophageal echocardiography. *Radiology* 2009; **250**: 61-67 [PMID: 19001153 DOI: 10.1148/radiol.2501080559]
54 **Olivares-Reyes A**, Chan S, Lazar EJ, Bandlamudi K, Narla V, Ong K. Atrial septal aneurysm: a new classification in two hundred five adults. *J Am Soc Echocardiogr* 1997; **10**: 644-656 [PMID: 9282354 DOI: 10.1016/s0894-7317(97)70027-0]
55 **Kuramoto J**, Kawamura A, Dembo T, Kimura T, Fukuda K, Okada Y. Prevalence of Patent Foramen Ovale in the Japanese Population- Autopsy Study. *Circ J* 2015; **79**: 2038-2042 [PMID: 26084379 DOI: 10.1253/circj.CJ-15-0197]
56 **Mas JL**, Arquizan C, Lamy C, Zuber M, Cabanes L, Derumeaux G, Coste J; Patent Foramen Ovale and Atrial Septal Aneurysm Study Group. Recurrent cerebrovascular events associated with patent foramen ovale, atrial septal aneurysm, or both. *N Engl J Med* 2001; **345**: 1740-1746 [PMID: 11742048 DOI: 10.1056/NEJMoa011503]

57 **Amat F**, Le Bret E, Sigal-Cinqualbre A, Coblence M, Lambert V, Rohnean A, Paul JF. Diagnostic accuracy of multidetector spiral computed tomography for preoperative assessment of sinus venosus atrial septal defects in children. *Interact Cardiovasc Thorac Surg* 2011; **12**: 179-182 [PMID: 21098509 DOI: 10.1510/icvts.2010.251298]

58 **Shovlin CL**. Pulmonary arteriovenous malformations. *Am J Respir Crit Care Med* 2014; **190**: 1217-1228 [PMID: 25420112 DOI: 10.1164/rccm.201407-1254CI]

Published by **Baishideng Publishing Group Inc**
7041 Koll Center Parkway, Suite 160, Pleasanton, CA 94566, USA
Telephone: +1-925-3991568
E-mail: bpgoffice@wjgnet.com
Help Desk: https://www.f6publishing.com/helpdesk
https://www.wjgnet.com